Eur. Phys. J. A **17**, 269–274 (2003)
DOI 10.1140/epja/i2002-10154-1

THE EUROPEAN PHYSICAL JOURNAL A

Low-energy photoproduction of Φ-mesons

J. Barth[1,a], W. Braun[1,b], J. Ernst[2], K.-H. Glander[1], J. Hannappel[1], N. Jöpen[1], F.J. Klein[1,b,c], F. Klein[1,d], H. Kalinowsky[2,b], E. Klempt[2], R. Lawall[1], J. Link[2,b], D. Menze[1], W. Neuerburg[1,b], M. Ostrick[1], E. Paul[1], H. van Pee[2], I. Schulday[1], W.J. Schwille[1], B. Wiegers[1,b], F.W. Wieland[1], J. Wißkirchen[1,b], and C. Wu[1]

[1] Physikalisches Institut, Bonn University, Bonn, Germany
[2] Helmholtz-Institut für Strahlen- und Kernphysik, Bonn University, Bonn, Germany

Received: 12 December 2002 /
Published online: 20 May 2003 –
Communicated by Th. Walcher

Abstract. Photoproduction of Φ-vector-mesons has been studied from reaction threshold up to $W = 2.4\,\mathrm{GeV}$ with the SAPHIR spectrometer at the Bonn electron stretcher ring ELSA. Total cross-sections, differential cross-sections and decay angular distributions were measured. We find evidence for strong non-diffractive contributions to Φ photoproduction.

PACS. 14.40.Cs Other mesons with $S = C = 0$, mass < 2.5 GeV

1 Introduction

Diffractive processes play an important role in hadronic collisions at high energies. In view of the hadronic structure of the photon, the photoproduction of vector mesons as described in the vector-meson dominance model is regarded as a key process to investigate diffractive scattering. The best investigated such reaction is the photoproduction of ϱ-mesons. For this process, F.J. Gilman *et al.* [1] already pointed to open questions concerning the interpretation of experimental results. The main problem is that the experiments indicate t-channel helicity violation, whereas s-channel helicity is conserved (see, *e.g.*, [2]). This implies a helicity flip in a t-channel picture. Thus one cannot assume a 0^+-particle exchange only, as expected in a naive picture for pure diffraction. Within the Regge model this implies that diffraction cannot be described by pomeron exchange alone.

One interesting question is how the experimentally determined cross-sections and angular distributions which are closely bound up with s- or t-channel helicity conservation continue or change towards lower energies. For photoproduction energies below 3 GeV a second equally interesting question arises: do hitherto unobserved resonances exist that couple weakly to the πN-channel but show up in vector-meson production? A couple of such resonances were predicted in quark-potential models [3–6].

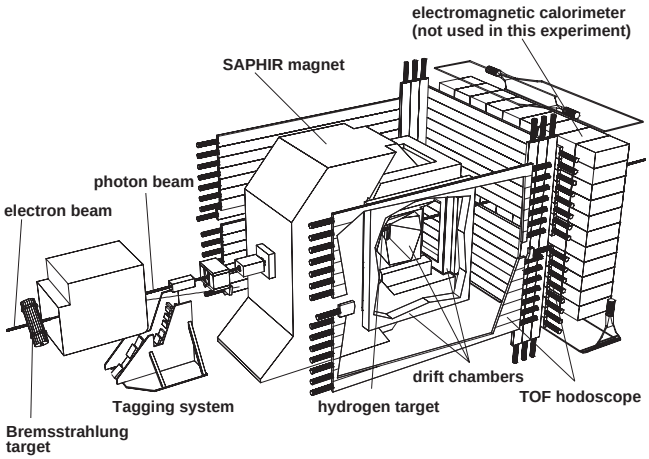

Fig. 1. Sketch of the SAPHIR detector.

V. Barger and B. Cline [7] pointed out that the photoproduction of Φ-mesons, due to its flavour contents, might be the ideal candidate to study "pure" diffraction and to determine the Pomeranchuk exchange amplitude. In their paper they present different predictions for the slope of the pomeron that could be determined by low-energy experiments. Within the discussion of our results, we will examine whether their conjectures are valid for energies below 3 GeV or whether other t-channel exchanges or s-channel resonances might contribute.

[a] Part of doctoral thesis.
[b] No longer working at this experiment.
[c] *Present address*: CUA, Department of Physics, Washington D.C., USA.
[d] e-mail: klein@physik.uni-bonn.de

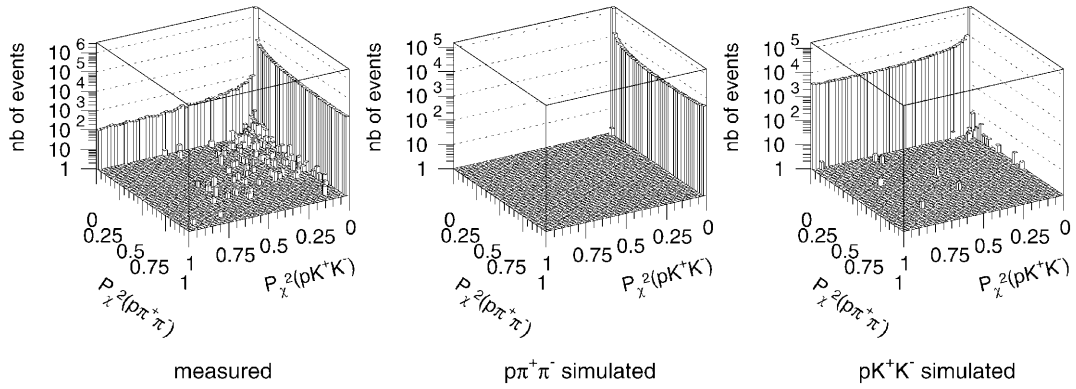

Fig. 2. Crosstalk histogram on the separation of pK^+K^- and $p\pi^+\pi^-$ final states.

2 Experimental method

The SAPHIR detector [8], shown schematically in fig. 1, is a multi-purpose magnetic spectrometer with a large angular acceptance consisting of a tagging facility, drift chambers and scintillator walls for triggering and time-of-flight measurements. The ELSA electron beam produces photons via bremsstrahlung in a copper foil target. The energies of the corresponding scattered electrons are determined in the tagging system for photon energies from 31% to 94% of the incident electron energy (up to 2.8 GeV). In coincidence with a photon counter behind the electromagnetic calorimeter (not visible in the figure) the tagging system also measures the effective photon flux passing through the liquid hydrogen target. It consists of a capton cylinder (8 cm long and 3 cm in diameter) and is surrounded by 14 cylindrical layers (partially stereo layers) of the central drift chamber, where all outgoing charged particles are detected. Their tracks are bent in the field of a C-shaped magnet which allows a measurement of momentum and charge. In forward direction a planar drift chamber ameliorates the momentum resolution. The surrounding scintillator wall determines the time of flight (TOF) of a particle and provides therefore, together with the measured momentum, information on its mass.

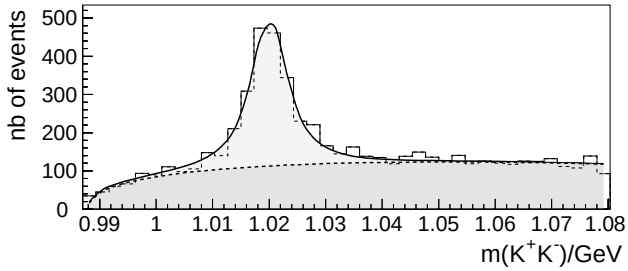

Fig. 3. Φ separation from the background in the K^+K^- mass spectrum.

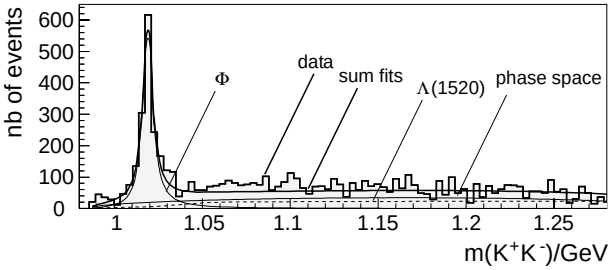

Fig. 4. Contributions of phase space, Λ(1520) and Φ production to the K^+K^- mass spectrum for photon energies between 2.1 and 2.4 GeV.

3 Data reduction and determination of the cross-sections

The available raw data (133 million events) stem from 3 data taking periods in 1997 and 1998 with an ELSA electron energy of 2.8 and 2.6 GeV, respectively. Hence photon energies vary from below reaction threshold up to 2.65 GeV. The trigger required two hits in the TOF wall together with a tagged photon in the tagging system. All triggered events are passed through a reconstruction software which delivers energy and momenta of the outgoing particles. The Φ-meson is detected by its decay into 2 charged kaons, therefore we look for pK^+K^- final states in our data. Starting from three prong events, we test various reaction hypotheses by kinematical fits, mainly: $\gamma p \to p\pi^+\pi^-$, $\gamma p \to pK^+K^-$, $\gamma p \to p\pi^+\pi^-\pi^0$, $\gamma p \to n\pi^+\pi^+\pi^-$, $\gamma p \to pK^+\pi^-$, $\gamma p \to pK^+\pi^-\pi^0$ and $\gamma p \to pe^+e^-$. For the analysis, those with the maximum value of the χ^2 probability for the kinematical fit of the pK^+K^- final state were selected. Figure 2 exemplarily shows the small contribution of crosstalk and misidentified events from $\gamma p \to p\pi^+\pi^-$.

Figure 3 shows the Φ signal in the K^+K^- mass spectrum above a continuous background. The only reaction which can be assigned clearly to the background is the production of the Λ(1520)-hyperon (decaying into pK^-). A fit of simulated Φ, Λ(1520) and phase space production data to the measured K^+K^- and pK^- mass spectra simultaneously (fig. 4) shows that the observed K^+K^- mass distribution is not satisfactorily described by the sum of these three contributions. Nevertheless, the fits indicate that the background is made up by Λ(1520) production to 50% at the Φ threshold, diminishing to about 20% at 2.5 GeV.

To separate the Φ signal from the background we therefore chose a phenomenological ansatz of the type

$bg(m) = c\cdot(m-a_1)^{b_1}\cdot(m-a_2)^{b_2}$ (where m is the invariant mass, c is a scale factor). The Φ signal function was fitted by a convolution of a Breit-Wigner shape with the natural decay width [9] and a Gaussian, reflecting the experimental resolution (Voigt function). The result is shown in fig. 3.

The acceptance of the detector was determined by Monte Carlo simulation. The generated particles were tracked through the SAPHIR detector by an adapted version of CERN's GEANT [10]. For a realistic simulation the detailed geometry of the detector and the measured efficiencies of drift chambers and scintillator hodoscopes were used.

In a first stage we generated Φ production events with an exponential slope $b = 4$ GeV^{-2} with respect to the squared transfered four-momentum $t = (p_p - p_{p'})^2 = (p_\gamma - p_\Phi)^2$ and a flat distribution in the Gottfried-Jackson system (see sect. 4). For each photon energy bin the acceptance was calculated for 5 or 6 bins in t between the respective kinematical limits $t_{\min}$ and $t_{\max}$. Based on these acceptance values, differential cross-sections and angular distributions were determined from experimental data. These results were used for a more realistic event generation in a second stage.

For very small generated $|t - t_{\min}|$, the proton gets a momentum too small to be detected and the acceptance approaches zero. Therefore, we evaluated the differential cross-sections starting from $|t - t_{\min}| \geq 0.01$ GeV^2. The cross-sections in the uncovered $|t - t_{\min}|$ range were determined by exponential extrapolation.

The systematic error caused by background separation is estimated to be approximately 10% for $\sigma_{\rm tot}$ and the slopes. The uncertainty resulting from the arbitrary choice of the t bins entering the exponential fit was checked by explicit variation and amounts to about 5% for $\sigma_{\rm tot}$ and 15% for the slopes. The systematic errors coming from flux normalization and target thickness are estimated to be less than 2% and 3%, respectively.

4 Results and interpretation

The differential cross-sections $\mathrm{d}\sigma/\mathrm{d}t$ were evaluated in four energy ranges. They are shown in fig. 5 together with an exponential fit of the form $\mathrm{d}\sigma/\mathrm{d}t = a\cdot\exp(-b|t-t_{\min}|)$. Within the errors of our measurement this exponential gives a fair description of the data indicating that t-channel exchange is dominant for t values corresponding to Φ production angles smaller than 90°. At larger angles the data hint at a possible deviation from this behaviour in accordance with the results from E. Anciant *et al.* [11] at 3.5 GeV photon energy. The total cross-section (fig. 6) was determined by integrating the exponential function from the t value of the fourth bin down to $|t - t_{\min}| = 0$ GeV^2 to extrapolate the behaviour of the cross-sections towards very small $|t - t_{\min}|$. The remaining bin(s) were added to account for possible deviations from the exponential behaviour at large $|t - t_{\min}|$.

Except for the threshold region, the resulting cross-section is relatively independent of the photon energy up to 2.6 GeV. The resulting slopes from the exponential fits are shown in fig. 7. In the photon energy range between 1.55 and 2.6 GeV, the slope parameter is relatively constant with a mean value of 2.5 GeV^{-2}. The data indicate a slight decrease with energy but this lies inside the statistical and systematic errors.

Decay angular distributions examine production mechanism hypotheses for vector mesons. Various reference systems are in common use. In the Gottfried-Jackson system (fig. 8), the quantization axis (z) is defined as the direction of the photon in the Φ rest frame. The direction of the

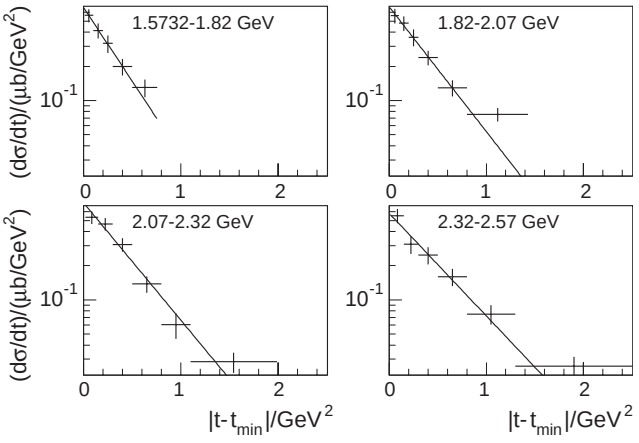

Fig. 5. Differential cross-sections $\mathrm{d}\sigma/\mathrm{d}t$.

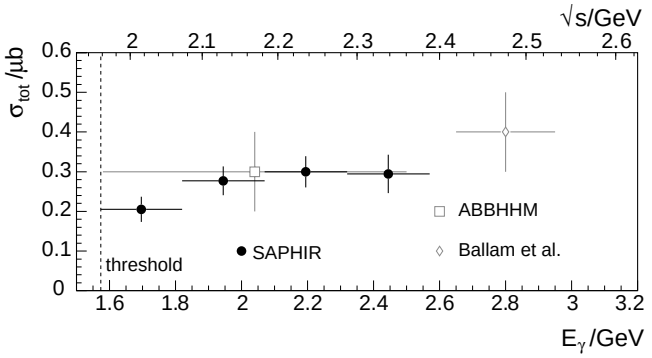

Fig. 6. Total cross section of the reaction $\gamma\mathrm{p} \to \mathrm{p}\Phi$ compared to results of earlier experiments [12,13].

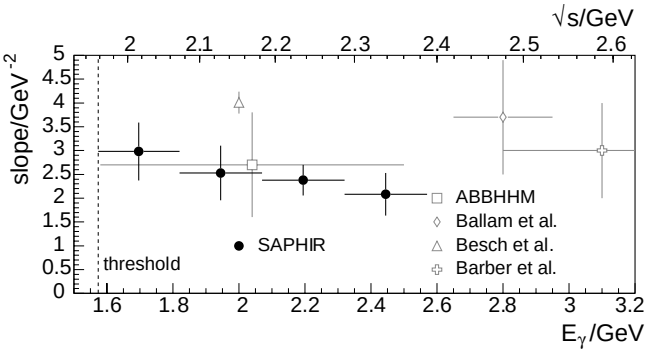

Fig. 7. Slope parameters b as a function of the photon energy E_γ, compared to results of earlier experiments [12–15].

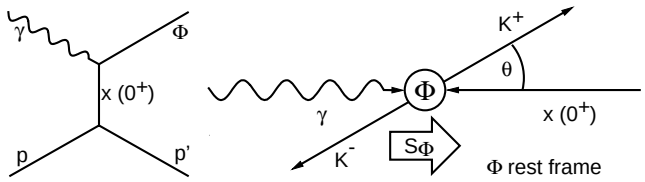

Fig. 8. The Gottfried-Jackson frame.

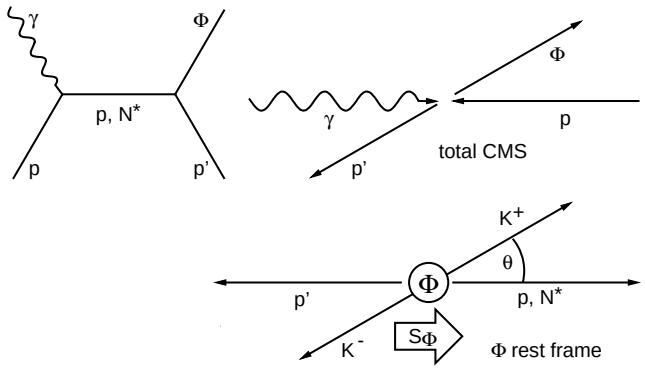

Fig. 9. The helicity frame.

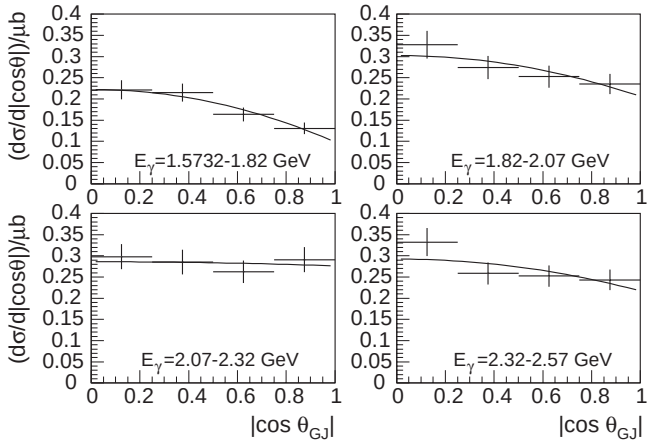

Fig. 10. Decay angular distributions in the Gottfried-Jackson frame.

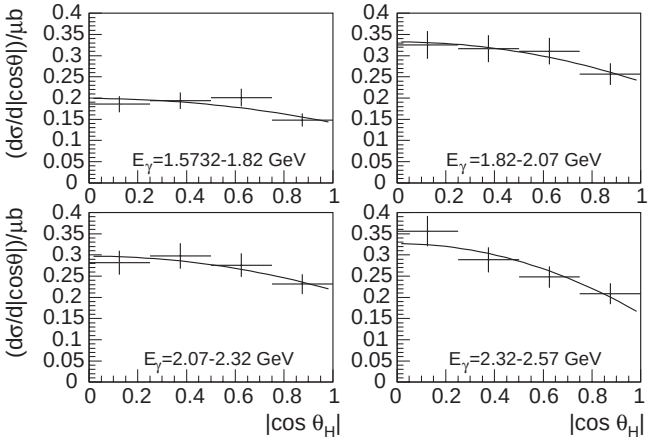

Fig. 11. Decay angular distributions in the helicity frame.

decay K^+ defines the polar angle θ, and the azimuthal angle φ with respect to the production plane. The Gottfried-Jackson system is used to test the "t-channel helicity" conservation which implies that the spin of Φ is aligned along the direction of the photon. "s-channel helicity" conservation is examined in the helicity system (fig. 9), here the quantization axis (z) points into the direction of Φ in the total CMS or opposite to the direction of the outgoing proton in the Φ CMS, respectively.

In both systems a $\sin^2\theta$ distribution for the decay K^+ is observed if the spin of Φ is aligned along the z-axis. The full decay angular distribution for Φ production with unpolarized photons can be expressed in terms of spin density matrix elements (see, *e.g.*, [16]):

$$W(\theta,\varphi) = \frac{3}{4\pi}\left(\frac{1}{2}(1-\varrho^0_{00}) + \frac{1}{2}(3\varrho^0_{00}-1)\cos^2\theta - \varrho^0_{1-1}\sin^2\theta\cos 2\varphi - \sqrt{2}\mathrm{Re}\varrho^0_{10}\sin 2\theta\cos\varphi\right).$$

We present decay angular distributions for $|\cos\theta|$ in both systems in figs. 10 and 11. Apparently, the four energy ranges exhibit similar shapes. We therefore evaluate the spin density matrix elements (table 1) and the φ and $\cos\theta$ distribution (figs. 12, 13) from all Φ-mesons over the full energy range in order to get a safer separation from background and smaller errors.

The observed Φ decay angular distributions in the helicity system differ noticeably from the results at higher energies, even from the data between 2.4 and 4.8 GeV [14] (fig. 14). All those experiments show "s-channel helicity" conservation, *i.e.* the θ_{H} distribution is well described by $\sin^2\theta_{\mathrm{H}}$ and the ϱ^0_{ik} are close to zero, respectively, in particular the ϱ^0_{00} which contains helicity flip amplitude contributions only. Besides the ϱ^0_{00}, also the $\varrho^0_{1-1} \approx 0.14$ is relatively large, indicating double helicity flip contributions. The energy independence of the angular distributions along with the exponential drop of $\mathrm{d}\sigma/\mathrm{d}t$ cross-sections excludes strong s-channel resonance contributions. Thus, probably t-channel exchanges of η and/or π^0 as well as a small quasi-continuous contribution from s-channel resonances in addition to diffractive production have to be taken into account.

The decay distributions in the Gottfried-Jackson system directly test diffractive production. The exchange of a 0^+ object in the t-channel (a pomeron within the Regge picture) would lead to a pure $\sin^2\theta_{\mathrm{GJ}}$ distribution; this is inconsistent with our results. Therefore, the conjecture of Barger and Cline [7] to determine the slope of the pomeron from low-energy Φ photoproduction is not valid.

At higher energies, decay angular distributions are available from the Daresbury experiment [14]. The curves in fig. 14 were generated by integrating the measured spin density matrix elements over all t bins. We observe that also in this energy range non-diffractive contributions appear. However, diffractive production is much more dominant than in our energy range and in the case of ϱ production (see, *e.g.*, [2]).

Table 1. Spin density matrix elements.

E_γ	Frame	ϱ^0_{00}	ϱ^0_{1-1}	$\mathrm{Re}\varrho^0_{10}$
1.573–2.57 GeV	Gottfried-Jackson	0.223 ± 0.018	0.0470 ± 0.0153	0.0531 ± 0.009
	Helicity	0.253 ± 0.021	0.140 ± 0.014	-0.0012 ± 0.01

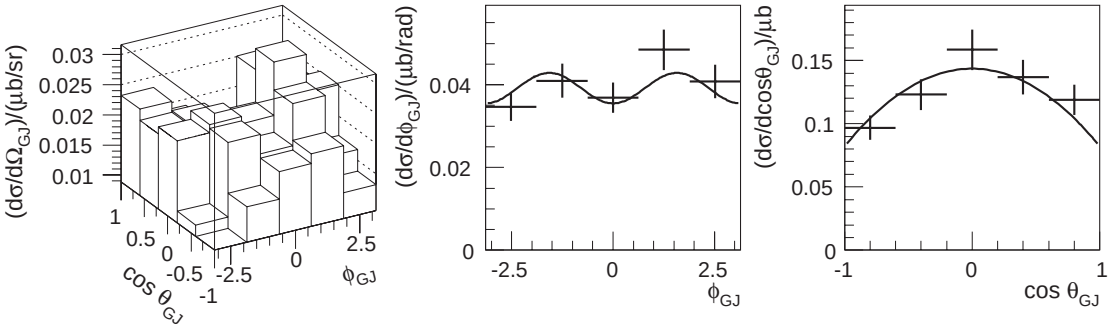

Fig. 12. Decay angular distributions in the Gottfried-Jackson frame.

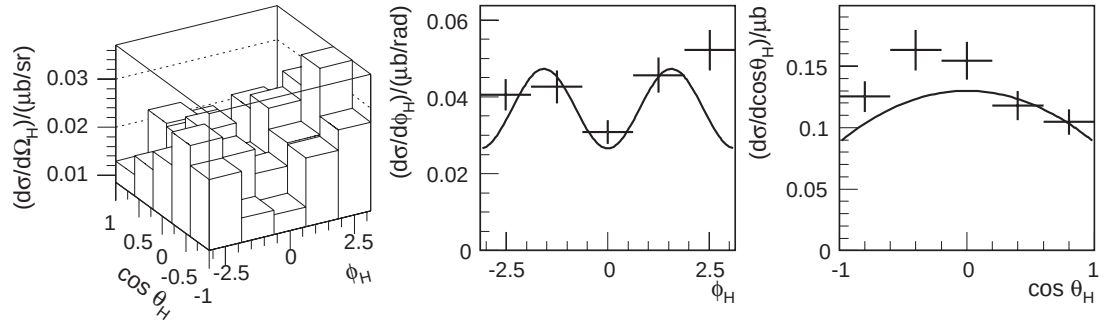

Fig. 13. Decay angular distributions in the helicity frame.

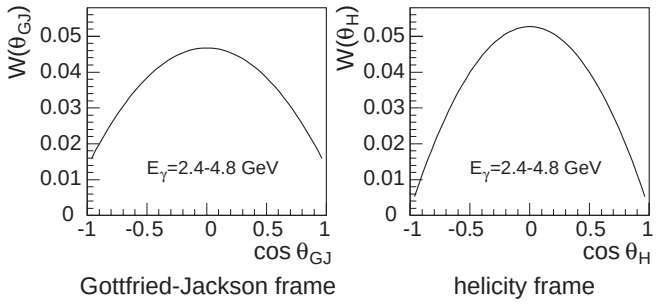

Fig. 14. Decay angular distributions in both Gottfried-Jackson and helicity frame evaluated from data in [14].

5 Summary

In summary, total and differential cross-sections and decay angular distributions were measured for the reaction $\gamma p \to \Phi p$ from threshold up to a photon energy of 2.6 GeV. Diffractive contributions (dominant at higher energies) are accompanied by non-diffractive terms. No indications for *s*-channel resonances are seen.

We gratefully acknowledge the help of the technical staff of the "Physikalisches Institut" and the engagement of the ELSA accelerator group. We would also like to thank Qiang Zhao (Department of Physics, University of Surrey, UK) for helpful discussions. This work is supported in part by the Deutsche Forschungsgemeinschaft (DFG) (SPP KL 980/2-3).

References

1. F.J. Gilman, J. Pumplin, A. Schwimmer, L. Stodolsky, Phys. Lett. B **31**, 387 (1970).
2. G. Wolf, *Photoproduction of Vector Mesons, Springer Tracts Mod. Phys.*, Vol. **59** (Springer, 1971) p. 77.
3. S. Capstick, N. Isgur, Phys. Rev. D **34**, 2809 (1986).
4. S. Capstick, W. Roberts, Phys. Rev. D **47**, 1994 (1993).
5. C.P. Forsyth, R.E. Cutkosky, Z. Phys. C **18**, 219 (1983).
6. R. Koniuk, N. Isgur, Phys. Rev. D **21**, 1868 (1980); Phys. Rev. Lett. **44**, 845 (1980); R. Koniuk, Nucl. Phys. B **195**, 452 (1982).
7. V. Barger, D. Cline, Phys. Rev. Lett. **24**, 23 (1970).
8. W.J. Schwille *et al.*, Nucl. Instrum. Methods Phys. Res. A **344**, 470 (1994).
9. Particle Data Group (D.E. Groom *et al.*), Eur. Phys. J. C **15**, 1 (2000) (URL: `http://pdg.lbl.gov`).
10. R. Brun, F. Carena *et al.*, GEANT Simulating Program for Particle Physics Experiments, Version 2.0, CERN DD/US/86.

11. E. Anciant *et al.*, Phys. Rev. Lett. **85**, 4682 (2000).
12. The Aachen-Berlin-Bonn-Hamburg-Heidelberg-München Collaboration, Phys. Rev. **175**, 1669 (1968).
13. J. Ballam *et al.*, Phys. Rev. D **7**, 3150 (1972).
14. D.P. Barber *et al.*, Z. Phys. C **12**, 1 (1982).
15. H.J. Besch *et al.*, Nucl. Phys. B **70**, 257 (1974).
16. K. Schilling, P. Seyboth, G. Wolf, Nucl. Phys. B **15**, 397 (1970).